A Two-Level Model for the Wind- and Buoyancy-forced Circulation*

RUI XIN HUANG

Department of Physical Oceanography, Woods Hole Oceanographic Institution, Woods Hole, Massachusetts

(Manuscript received 6 June 1991, in final form 23 March 1992)

ABSTRACT

The classic theory of deep circulation by Stommel and Arons is extended to a two-level model. Instead of specifying the interfacial upwelling a priori, it is calculated as part of the solution. The model shows strong upwelling along the southern and eastern boundaries, while the upwelling in the interior ocean is much weaker. With a medium rate of Ekman pumping, the basin is separated into western and eastern regions by critical characteristics. It is shown that across the boundary between the different regions temperature and velocity are continuous, but vorticity (or some higher-order quantity) is discontinuous.

1. Introduction

Theories of deep circulation can be traced back to the classical work by Stommel and Arons (1960) in which they studied a pie-shaped basin with a prescribed uniform upwelling everywhere. Their model provided a kinematic view of the deep circulation. There seems to be no reason, a priori, however, that the upwelling should be uniform throughout the basin. A rather surprising result from the model is that, due to the kinematic constraint of the model, water in the ocean interior is actually moving toward the source. While offering an interesting flow pattern of the deep circulation, the model is unable to make the link between the deep flow and the forcing on the sea surface.

In the 1970s much effort was spent on finding some similarity solutions of thermocline–thermohaline circulation. Although similarity solutions can provide useful information about the circulation, they cannot satisfy some of the essential boundary conditions for the circulation in a closed basin. Thus, recent studies have been focused on nonsimilarity solutions. There are numerous publications relating to this topic, and it is almost impossible to list all the contributions; for a comprehensive review on this topic, see Huang (1991). Since the model is analytical or quasi-analytical, a few papers that seem more relevant, however, will be quoted.

In a study of the subtropical front, Cushman-Roisin (1984) derived and solved a first-order partial differential equation for the surface temperature by using characteristic coordinates. The present model is similar to his but much simpler. Killworth (1985) discussed a two-level numerical model that is very close to the present model. The major difference is the assumption of uniform lower-layer temperature in the present model, which allows simple analytical solution. In comparison, strong diffusion required for numerical stability makes numerical models rather hard to understand. For the circulation driven by combined wind- and buoyancy forcing, Luyten and Stommel (1986) derived a similar equation for the layer depth by specifying the interfacial mass flux. They also gave a detailed discussion about the physical meaning of the characteristics and the direct/indirect cells in the subpolar basin. To describe the singular (saddle) point where the characteristics coming from different dynamical regions meet, a point called the Rossby repellor was first introduced. Pedlosky (1986) discussed a three-moving-layer model for a subtropical basin using a similar technique. These models are designed for the ocean interior, while the dynamical structure of the relevant boundary currents of a single (deep) moving layer was discussed in some detail by Kawase (1987).

A common approach in these models is to parameterize the interfacial upwelling/downwelling velocity in simple ways, that is, by specifying it as a constant, a linear function of latitude, or some other simple function. In some sense it is very much like the similarity approach; that is, specifying the interfacial mass flux implies some constraints on the solution, which may be unrealistic. One of our goals in this study is to build a simple model in which the vertical velocity is generated through internal dynamics, such as the ther-

* Contribution Number 7771 from the Woods Hole Oceanographic Institution.

Corresponding author address: Dr. Rui Xin Huang, Department of Physical Oceanography, Woods Hole Oceanography Institution, Woods Hole, MA 02543.

mal wind relation and the planetary vorticity equation. The model is set up in spherical coordinates in section 2. Two cases will be discussed; the first case with no wind forcing and the second case with a medium size of Ekman pumping.

2. The model

The ocean is represented by a two-level model in spherical coordinates. Both layers have the same constant thickness h. The ocean is forced from above by a Rayleigh type of buoyancy forcing; that is, the thermal boundary condition is parameterized in terms $F = \gamma(T^* - T)$, where γ is a relaxation constant and T^* is the reference temperature. This parameterization was introduced by Haney (1971). According to his analysis, air–sea heat flux, including the incoming solar radiation, longwave radiation, and latent heat flux, can be parameterized as a heat flux due to relaxation to a reference temperature. By appropriate choice of the reference temperature and the relaxation constant, this parameterization can give air–sea heat exchange close to observations.

Two cases will be considered: one is purely buoyancy driven and the other is driven by Ekman pumping w_e combined with buoyancy forcing. At each location the air–sea heat flux is balanced by cold water upwelling and horizontal heat advection; see Fig. 1. The deep-water formation in the northeast corner feeds the basinwide upwelling. Instead of specifying a basinwide uniform upwelling as in the Stommel and Arons (1960) model, the upwelling velocity will be calculated as part of the solution. As a result of this upwelling, the upper layer moves southward and the lower layer moves northward. A no-zonal-flow condition at the eastern boundary gives rise to an anticyclonic gyre in the upper layer and a cyclonic gyre in the lower layer. (In addition, if Ekman suction is applied to the subpolar basin, there is also a cyclonic gyre in the upper layer.) As in the Stommel and Arons (1960) model, a loop of boundary currents is proposed in order to close the mass transport.

In a model without friction or inertial terms in the momentum equations, the no-zonal-flow condition could be applied to either the eastern or the western walls; thus, a southward motion might give rise to either a cyclonic gyre or an anticyclonic gyre. If friction or inertial terms are included, however, it can be readily shown that only the western boundary layer is dynamically consistent, so the no-zonal-flow condition should apply to the eastern boundary. The details of the boundary currents depend on the dynamical assumptions made for these currents. Since the focus of this study is on the interior dynamics, the no-zonal-flow condition is assumed to be valid along the eastern boundary of the model without going through the details of the boundary-layer analysis.

Notice that an important assumption will be made

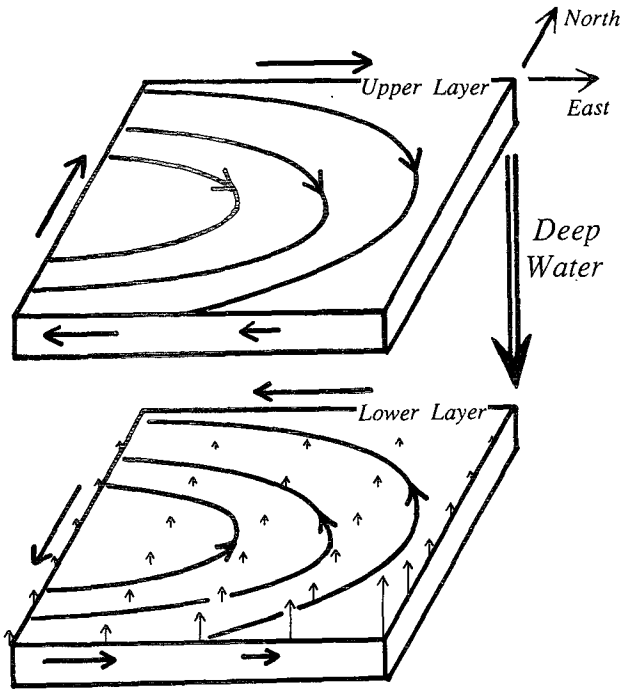

FIG. 1. A schematic view of a thermally forced model ocean. Heavy arrows and lines indicate an anticyclonic gyre in the upper layer and a cyclonic gyre in the lower layer. Deep water is formed in the northeastern corner and sinks to the lower layer. Heavy arrows along the edge of the basin depict the boundary currents required for mass transport. Thin arrows indicate the cold water upwelling.

that there is only one source of deep water. Therefore, the lower layer has a constant temperature T_b, while the temperature in the upper layer varies horizontally. This assumption makes the model much simpler; however, this assumption has to be examined at the end of our calculation in order to make sure that the model is self-consistent.

Basic equations of the model include geostrophy for the horizontal velocity, hydrostatic equilibrium, continuity, and heat balance,

$$-2\omega \sin\theta v = -\frac{1}{\rho_0 r \cos\theta}\frac{\partial p}{\partial \phi}, \tag{1}$$

$$2\omega \sin\theta u = -\frac{1}{\rho_0 r}\frac{\partial p}{\partial \theta}, \tag{2}$$

$$\frac{\partial p}{\partial z} = -\rho g, \tag{3}$$

$$\frac{1}{r\cos\theta}\left[\frac{\partial}{\partial\theta}(v\cos\theta) + \frac{\partial u}{\partial\phi}\right] + \frac{\partial w}{\partial z} = 0, \tag{4}$$

$$\frac{1}{r\cos\theta}\left[\frac{\partial}{\partial\theta}(vT\cos\theta) + \frac{\partial}{\partial\phi}uT\right] + \frac{\partial}{\partial z}wT = \frac{\partial F}{\partial z}, \tag{5}$$

where ω is the earth's angular velocity of rotation, u, v, w are the velocity components, r is earth radius, p

is the pressure, and ρ_0 is the reference density. The turbulent heat flux F is assumed to be zero at the interface and bottom. Water density is a linear function of temperature

$$\rho = \rho_0(1 - \alpha T), \tag{6}$$

where α is the thermal expansion coefficient. The thermal wind relations can be derived from (1, 2, 3, 6):

$$2\omega \sin\theta \frac{\partial v}{\partial z} = \frac{\alpha g}{r \cos\theta} \frac{\partial T}{\partial \phi}, \tag{7}$$

$$2\omega \sin\theta \frac{\partial u}{\partial z} = \frac{-\alpha g}{r \cos\theta} \frac{\partial T}{\partial \theta}. \tag{8}$$

By cross differentiating (1, 2) and substituting into (3), the vorticity equation is obtained:

$$v = r \tan\theta \frac{\partial w}{\partial z}. \tag{9}$$

All these equations are valid for a continuously stratified ocean. In this study these equations will be applied to the two-level model ocean. Using the vorticity equation (9) to the upper layer, the vertical velocity at the interface is

$$w^* = w_e - \frac{\cot\theta h}{r} v_1, \tag{10}$$

where w_e is the Ekman pumping velocity imposed on the upper surface and v_1 is the meridional velocity in the upper layer.

Applying the vorticity equation (9) to both layers, a relation for the barotropic mass flux is obtained,

$$h(v_1 + v_2) = r \tan\theta w_e, \tag{11}$$

where the lower boundary condition of $w = 0$ has been used.

In the following analysis the subscript 1 for the upper layer will be dropped. Note that the mean temperature gradient at the interface is one-half of that in the upper layer. From (7) and (11) the meridional velocity in the upper layer is

$$v = \frac{\alpha g h}{8 r \omega \sin\theta \cos\theta} \frac{\partial T}{\partial \phi} + \frac{r}{2h} \tan\theta w_e. \tag{12}$$

The first part is the baroclinic velocity due to the horizontal temperature gradient, and the second part is the barotropic velocity due to the Ekman pumping.

The interfacial upwelling velocity is

$$w^* = \frac{1}{2} w_e - \frac{\alpha g h^2}{8 r^2 \omega \sin^2\theta} \frac{\partial T}{\partial \phi}. \tag{13}$$

The first part is clearly due to the Ekman pumping; the second part is due to the baroclinic effect.

The zonal velocity can be calculated by zonally integrating the continuity equation, and applying the no zonal velocity condition at the eastern wall, and the result is

$$u = -\frac{\alpha g h}{8 r \omega \sin\theta} \frac{\partial T}{\partial \theta} - \frac{r \cos\theta}{h} \left(w_e + \frac{\tan\theta}{2} \frac{\partial w_e}{\partial \theta} \right) (\phi - \phi_e), \tag{14}$$

where ϕ_e is the eastern boundary.

Using these equations and integrating (5) over the upper layer, a first-order partial differential equation for T is obtained:

$$u_c \frac{\partial T}{\partial \phi} + v_c \frac{\partial T}{\partial \theta} = \frac{w_e}{2} (T_b - T) + \gamma (T^* - T), \tag{15}$$

with

$$u_c = a(T_b - T) - b(\phi - \phi_e),$$

$$a = \frac{\alpha g h^2}{8 r^2 \omega \sin^2\theta}, \quad b = w_e + \frac{\tan\theta}{2} \frac{\partial w_e}{\partial \theta}, \tag{16}$$

$$v_c = \frac{\tan\theta}{2} w_e. \tag{17}$$

This equation is very similar to the equation used by Luyten and Stommel (1986). The solution of this equation will be discussed in detail in section 4.

3. A case of purely thermal forcing

Since w is zero at the sea surface and at the bottom, the barotropic meridional and zonal mass flux are zero, and the velocity in the upper layer is

$$u = -\frac{\alpha g h}{8 r \omega \sin\theta} \frac{\partial T}{\partial \theta},$$

$$v = \frac{\alpha g h}{8 r \omega \sin\theta \cos\theta} \frac{\partial T}{\partial \phi},$$

$$w^* = -\frac{\alpha g h^2}{8 r^2 \omega \sin^2\theta} \frac{\partial T}{\partial \phi}. \tag{18}$$

Thus, the isotherms are the geostrophic contours; that is,

$$u \frac{\partial T \cos\theta}{\partial \theta} + v \frac{\partial T}{\partial \phi} = 0.$$

The heat equation (15) is reduced to a simple balance between the upwelling and the air–sea interaction

$$w^*(T - T_b) = \gamma (T^* - T). \tag{19}$$

Since the latitude coordinate appears only as a parameter implicitly, this equation is simply an ordinary differential equations for $dT/d\phi$, and its solution is

$$\frac{8 \gamma r^2 \omega \sin^2\theta}{\alpha g h^2} (\phi - \phi_e) = T - T_e + (T^* - T_b) \ln \frac{T^* - T}{T^* - T_e}. \tag{20}$$

In this study the reference temperature is assumed to be a linear function of latitude

$$T^* = T_s + (T_n - T_s)\cdot\frac{\theta - \theta_s}{\theta_n - \theta_s}, \qquad (21)$$

where $T_s = 15°C$, $T_n = 2°C$, $\theta_s = 0°N$, and $\theta_n = 70°N$. The eastern and western boundaries of the model basin are located at 0° and 60°W. The air–sea interaction coefficient $\gamma = 0.07$ m day$^{-1} \approx 8.1 \times 10^{-5}$ cm s^{-1}. The thickness of both layers is $h = 500$ m. Since the zonal velocity vanishes along the eastern boundary, T must be constant. In this study it is set to

$$T_e = 2°C, \quad T_b = 0°C. \qquad (22)$$

The basic stratification along the eastern boundary, $T_e - T_b$, is chosen somewhat arbitrarily. In the oceans both T_e and T_b are determined by global dynamic balance, which is not simulated explicitly in the model.

The upper-layer temperature, also the geostrophic contours, shows an anticyclonic gyre in the upper layer (Fig. 2a). This temperature is maintained by a balance between the air–sea interaction, horizontal advection, and the cold water upwelling. The model's results show strong upwelling along the eastern boundary and the southern boundary, while the upwelling in the interior ocean is at least 10 times less (Fig. 2b).

The higher rate of upwelling along the eastern and southern boundaries is due to the lowest temperature there. A physical explanation is straightforward. The interfacial upwelling drives a southward flow, and to conserve mass water, must return northward somewhere along the boundaries of the basin. The meridional gradient of the ambient planetary vorticity, the β term in the vorticity equation, determines, however, that this return flow must be near the western wall, instead of the eastern wall. Thus, there is an anticyclonic gyre in the upper layer. Following the geo-

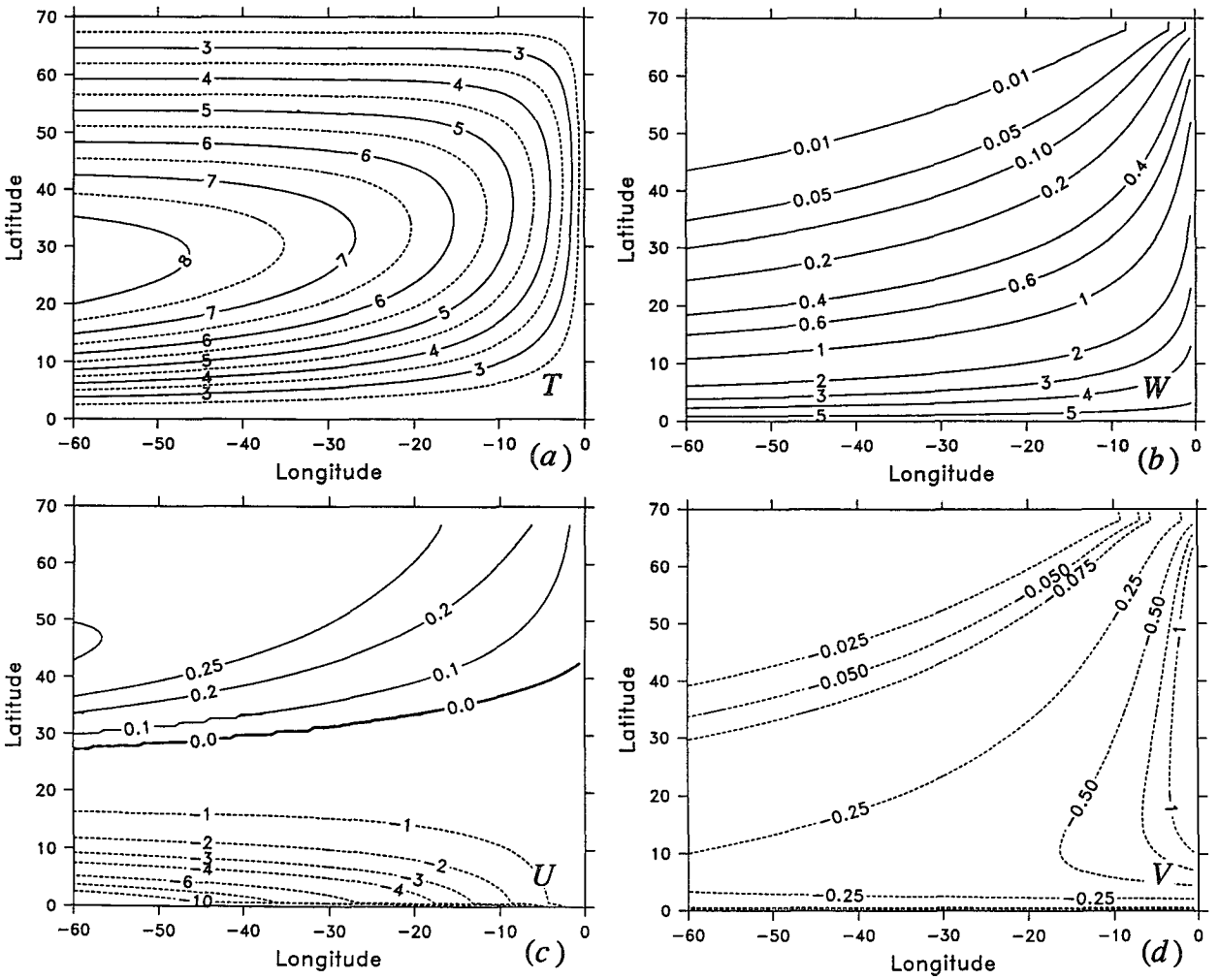

FIG. 2. Solution of a case of purely thermal forcing, $T_b = 0°C$ and $T_e = 2°C$. (a) T (°C), (b) w^* in 10^{-4} cm s^{-1}, and (c) u and (d) v in centimeters per second.

strophic relation, temperature is the lowest along the eastern and southern walls. From (19), the upwelling rate is determined by $\gamma(T^* - T)/(T - T_b)$, so it is stronger at the eastern boundary compared with the interior. Along the eastern boundary the upwelling rate increases southward due to increase in T^*. At the equator the upwelling rate reaches its maximum. Note that the maximum upwelling rate is linearly proportional to the relaxation constant γ. One may notice that the relaxation constant used here, 0.07 m day^{-1}, is 10 times smaller than the value, 0.7 m day^{-1}, recommended by Haney (1971). The motivation of choosing a small γ is to limit the strength of upwelling, especially near the equator, and to reproduce a thermohaline circulation whose strength is comparable to observations.

Since the upwelling is finite at the equator, the meridional velocity vanishes there. Therefore, the equator is not a singular latitude for the model. In fact, these maps are based on calculations in which the southernmost grids are located at 0.01°N. Accordingly, no equatorial boundary layer is required for the model.

Higher upwelling near the eastern boundary of the model is consistent with an upwelling rate for the oceans estimated by simple scaling of $w \approx k/d$, where k is the vertical diffusivity and d is the scale depth of the main thermocline. Since isopycnals near the eastern boundary are closely packed near the upper surface, the upwelling velocity w is larger near the eastern boundary. The stronger upwelling along the southern boundary is well known from observations and many models.

The meridional velocity is large along the eastern boundary and off the equator, as seen in Fig. 2d. Apparently, the interior solution does not satisfy the lateral boundary conditions along the western wall. To close the circulation there must be a loop of boundary currents along the western edge of the model basin (Fig. 3). Starting from the southwestern corner, the mass flux of the western boundary increases to 47.6 Sv (Sv $\equiv 10^6$ m^3 s^{-1}). In the northern part of the western boundary, as some water is recirculated through the eastward flow out of the western boundary current, the mass flux in the western boundary current declines to 41.9 Sv. Within the northern boundary current, the mass flux remains practically constant.

Notice that deep-water formation is not included in the model. For one thing, the coldest reference temperature is higher than the abyssal temperature; thus, formation and sinking of such cold water is impossible within the model. The dynamic details of the western boundary layer and the deep-water formation process, which drives the circulation described here, are left for further study.

4. A case with Ekman pumping

It is interesting to study the case with Ekman pumping, which is used to simulate the wind-stress curl. In this section the focus is on the interaction between the thermal forcing and the wind-stress-induced Ekman pumping. The ocean is forced with Ekman pumping in the south and Ekman suction in the north

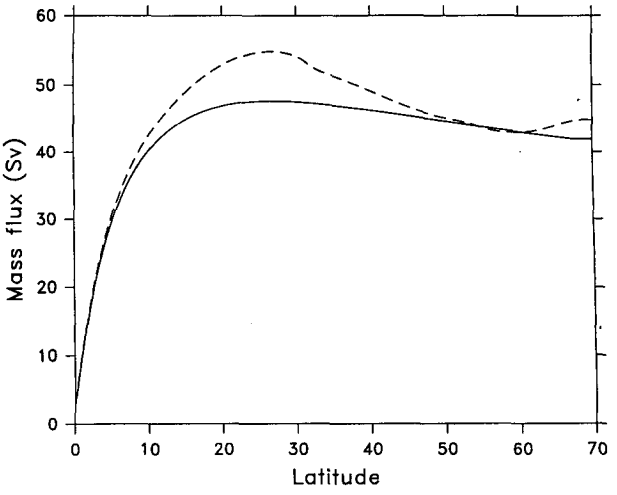

FIG. 3. Mass transport within the boundary currents. The solid line is for a case without Ekman pumping; the dashed line for a case with Ekman pumping.

$$w_e = w_0 \sin\left(2\pi \frac{\theta - \theta_s}{\theta_n - \theta_s}\right), \tag{23}$$

where $w_0 = -0.35$ cm $\times 10^{-4}$ s^{-1}.

Solution of this case can be calculated by integrating (15), which is a first-order partial differential equation in characteristic form for T, similar to an equation used by Luyten and Stommel (1986). The characteristics are defined by $dx/ds = u_c$, $dy/ds = v_c$. The meridional characteristic velocity is entirely due to the wind-stress steering. The zonal characteristic velocity u_c consists of two terms: the first term is the layer-integrated baroclinic velocity due to the vertical temperature difference and the second term is the layer-integrated barotropic velocity due to Ekman pumping. Notice that both terms are zero at the eastern boundary; however, a small distance away from the eastern boundary these two terms are nonzero. Mathematically, the eastern boundary is a singular solution for the characteristic equation. In fact, the eastern boundary itself is both a characteristic and a streamline. Moreover, there are many characteristics tangential to the eastern boundary that flow to the basin interior. Physically, these characteristics cover the eastern region of the basin, and the influence of the eastern boundary condition is propagated westward along these characteristics.

As one moves westward in the ocean interior, the barotropic velocity term in the zonal characteristic velocity increases gradually. Eventually, along a special line, the zonal characteristic velocity vanishes and characteristics started from the eastern boundary (the

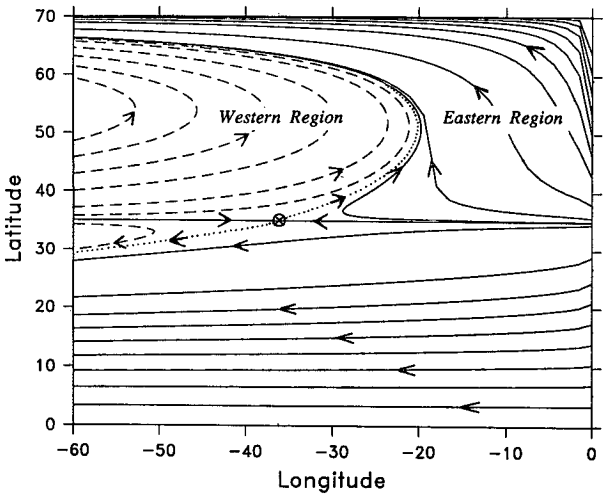

FIG. 4. Schematic pattern of characteristics for the case with Ekman pumping. A crossed circle in the middle indicates the Rossby repellor, which is a saddle point for the characteristics. Two characteristics, depicted by dotted lines, separate both the subpolar and subtropical basin into the eastern and western regions.

so-called eastern characteristics) go back eastward. Therefore, there is a certain domain that must be covered by characteristics stemming from the western boundary (the so-called western characteristics), instead of eastern characteristics. There are two special characteristics, one from the eastern boundary and the other from the western boundary. At a point in the midocean (the so-called Rossby repellor) these two characteristics meet and bifurcate into two new characteristics, one going poleward and the other equatorward. These two characteristics define the boundary separating the basin into the eastern and western regions, both of which are covered by characteristics begun from the eastern boundary or the western boundary, as shown in Fig. 4.

The eastern boundary condition is the same as before; that is, $T_e = 2°C$. The bottom temperature T_b is set to be 0°C. As discussed in the preceding section, this choice of T_b is somewhat arbitrary. In a more complex model, T_b should be determined by the global heat balance, and could be different for these two cases.

For the amount of Ekman pumping applied, a substantial part of the subpolar basin is covered by western characteristics. For calculation along these characteristics the initial temperature condition at the western boundary is required. In the model this temperature can be specified fairly arbitrarily. (This is certainly the weakest part of the model, due to the lack of boundary-layer dynamics.) In this study a constant temperature $T_{wc} = T_{ws} - 1.0$ has been chosen as the western boundary condition for western characteristics, where T_{ws} is the temperature at the western wall of the northernmost characteristic belonging to the eastern region of the subtropical basin. Obviously, given all other parameters, a different choice of the temperature condition for western characteristics will certainly lead to different solutions within the western regions. One reason for the specific temperature condition chosen for the western characteristics, however, is to avoid possible downwelling within western regions. As discussed in the model formulation, a single source of deep water is an essential condition for the model to be self-consistent. Downwelling within the western region can give rise to two sources of deep water and thus lead to an inconsistency of the model.

Before presenting the solution, the structure in the vicinity of the Rossby repellor is examined. Along the intergyre boundary $\theta = \theta_R$ the Ekman pumping velocity vanishes, so the characteristic is zonal. Equation (15) is reduced to

$$[a(T_b - T) - b(\phi - \phi_e)]\frac{dT}{d\phi} = \gamma(T^* - T), \quad (24)$$

where both a and b, defined in (16), are positive. The general solution of this equation is

$$(\gamma - b)\left[\phi - \phi_e + \frac{a}{b}(T^* - T_b)\right] = C|T^* - T|^{b/\gamma} - a(T^* - T), \quad (25)$$

where C is a constant, which can be determined from the temperature boundary condition at the eastern/western wall. The Rossby repellor is located at

$$\phi_R = \phi_e - \frac{a}{b}(T^* - T_b), \quad \text{where } T = T^*. \quad (26)$$

Using the corresponding parameters, the Rossby repellor for the present model is located at 41°W. Notice that the position of the Rossby repellor depends on Ekman pumping and the bottom-layer temperature. Although temperature is continuous at the Rossby repellor, this is really a singular point for the solution. Since (25) is continuous for $\phi > \phi_R$ or $\phi < \phi_R$, by differentiating the one-sided derivatives at ϕ_R with respect to ϕ,

$$T_\phi(\phi_R, \theta_R) = 0, \quad \text{if} \quad b/\gamma \leqslant 1$$
$$= \frac{\gamma - b}{a}, \quad \text{if} \quad b/\gamma > 1$$
$$T_{\phi\phi}(\phi_R, \theta_R) = -\infty, \quad \text{if} \quad 1/2 < b/\gamma < 2$$
$$= 0, \quad \text{if} \quad b/\gamma < 1/2 \quad \text{or} \quad b/\gamma > 2.$$

Note that these expressions are valid for both $\phi \to \phi_R^+$ and $\phi \to \phi_R^-$. Thus, T_ϕ is actually continuous at ϕ_R. When $b/\gamma = 1/2$ or 2, $T_{\phi\phi}(\phi_R, \theta_R)$ is finite on each side of ϕ_R but has different values.

Similarly, $T_{\phi\phi\phi}(\phi_R, \theta_R)$ is unbounded within region of $1/3 < b/\gamma < 3$, but it vanishes for $b/\gamma < 1/3$ or $b/\gamma > 3$.

Basically, ϕ_R is an essential singular point for Eq. (24), so solutions on either side of ϕ_R cannot com-

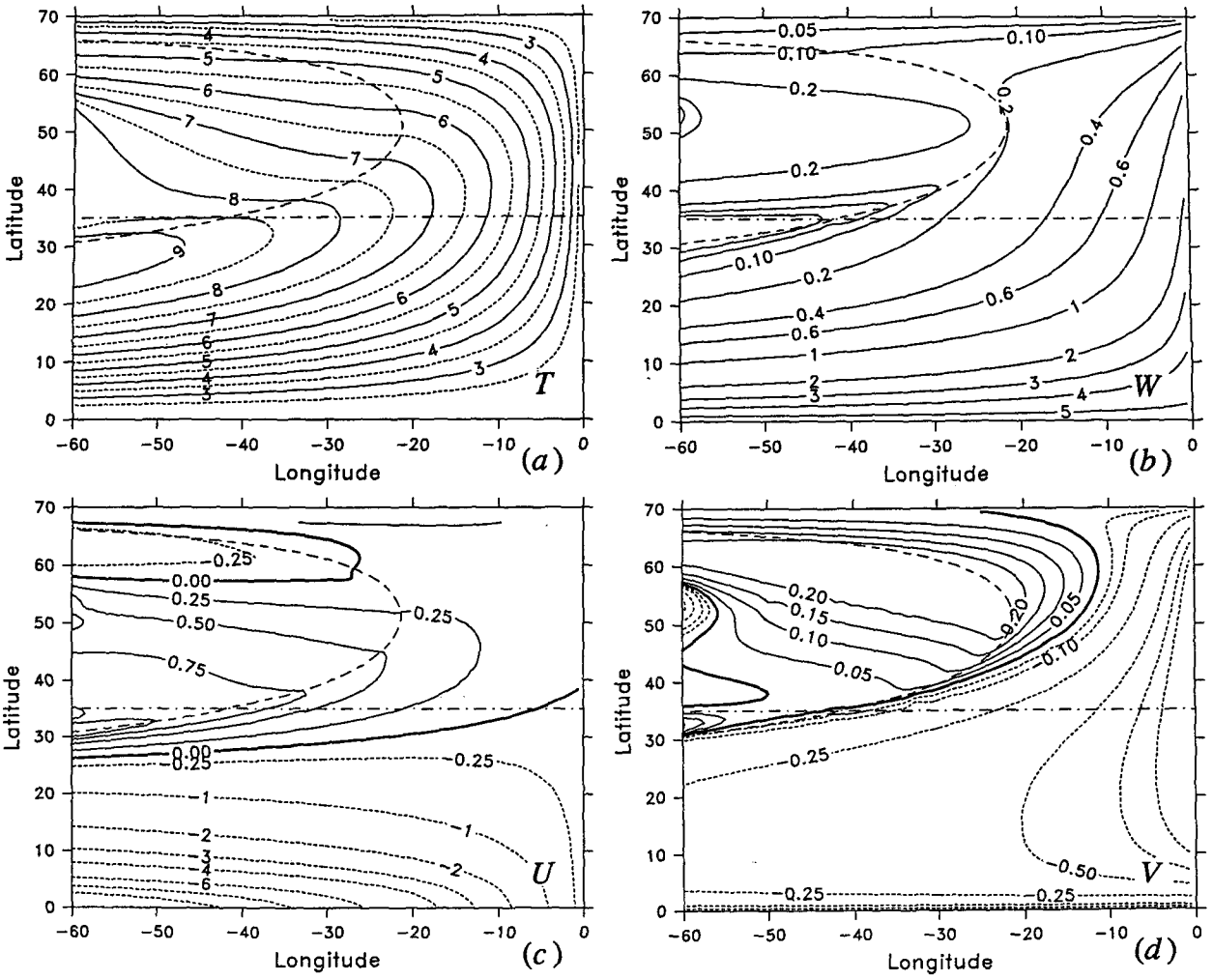

FIG. 5. Solution of a case with Ekman pumping, $T_b = 0°C$ and $T_e = 2°C$. The dashed line separates the eastern and western regions, and the dashed-dotted line is the intergyre boundary. (a) T in degrees Celsius, (b) w^* in 10^{-4} cm s^{-1}, and (c) u and (d) v in centimeters per second. Notice that the meridional velocity should have been zero at the Rossby repellor. Smoothing in contouring routines, however, distorted the pattern near the Rossby repellor.

municate with each other. This is just another way of saying that west of the repellor characteristics come from the western boundary, and the solution is independent of that in the eastern region.

There are two critical characteristics starting from the Rossby repellor, which separates the subtropical/subpolar basin into two regions: an eastern region and a western region (Fig. 4). Since boundary conditions for these two regions can be quite different, there is possibly some kind of discontinuity across this critical characteristic. A close examination reveals, however, that temperature and its first derivative (the velocity fields) are actually continuous (Fig. 5). This can be shown by the following analysis. The boundary conditions within each region are assumed to be continuous. Within each region, therefore, the solution is continuous and differentiable. Differentiating (15) with respect to ϕ, one obtains

$$u_c \frac{\partial}{\partial \phi}\left(\frac{\partial T}{\partial \phi}\right) + v_c \frac{\partial}{\partial \theta}\left(\frac{\partial T}{\partial \phi}\right) = F \cdot \frac{\partial T}{\partial \phi}, \qquad (27)$$

where F is a function independent of $\partial T/\partial\phi$. Notice that in deriving this relation, the facts that both w_e and T^* are independent of ϕ have been used. For the case under discussion, $b/\gamma = 0.83$, so $T_\phi(\phi_R, \theta_R) = 0$, $T_{\phi\phi}(\phi_R, \theta_R) = -\infty$. Since $\partial T/\partial\phi$ is zero at the Rossby repellor, it remains zero along characteristics begun at the repellor. However, $T_{\phi\phi}$ is unbounded along these two characteristics. Therefore, the boundary between the eastern and western regions is a vorticity front.

Notice that our solution is valid only within the region where

$$T_b \leqslant T^*.$$

This can be shown by the following. For simplicity, three special latitudes will be discussed where $w_e = 0$.

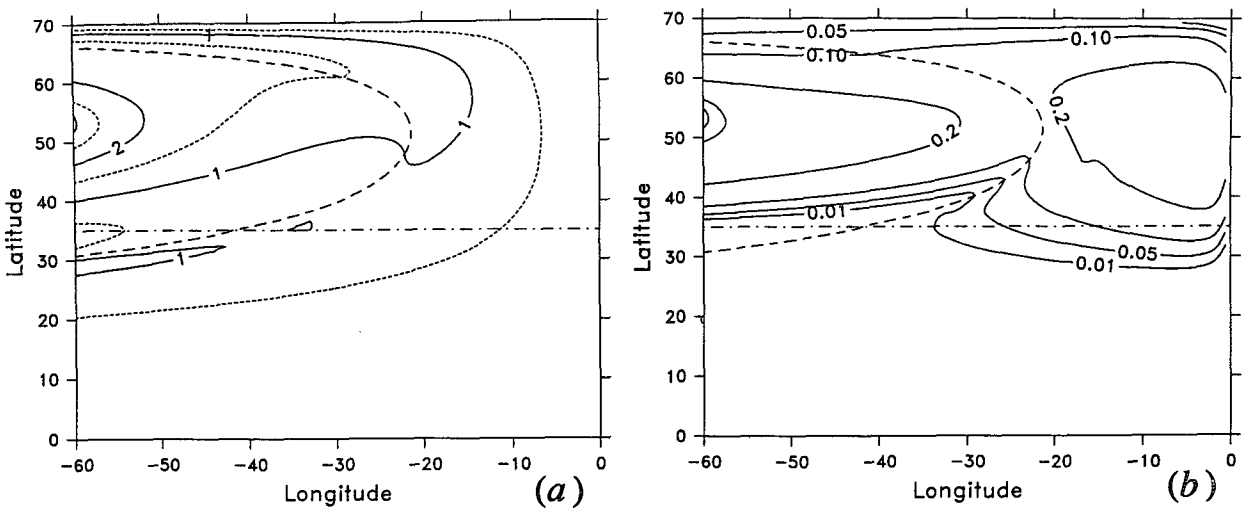

FIG. 6. Difference between cases with and without Ekman pumping: (a) Temperature (°C) and (b) upwelling velocity at the interface in 10^{-4} cm s^{-1}.

At the eastern wall $dT/d\phi = \infty$, or $d\phi/dT = 0$. A simple manipulation gives

$$\frac{d^2\phi}{dT^2} = -\frac{a}{\gamma(T^* - T_e)}. \tag{28}$$

Therefore, if $T_e < T^*$,

$$\Delta\phi = \frac{1}{2}\frac{d^2\phi}{dT^2}\Delta T^2 < 0. \tag{29}$$

This means the characteristics begun at the eastern wall will go westward; however, if $T_e > T^*$, $d^2\phi/dT^2 > 0$, so characteristics started from the eastern boundary will go eastward; that is, this part of the solution cannot be determined from the eastern boundary condition. Thus, we will ignore a small strip of area near the northern wall where $T_e > T^*$. This can be treated as the place where the deep water is formed and sinks to the second layer; the dynamic detail of this region is not included in this simple model.

Within the subpolar basin the upper-layer water is much warmer in the case with Ekman pumping, compared with that of no wind forcing. The difference is especially profound within the western region. This reflects the different nature of the solution. Physically, wind-stress curl introduces a strong eastward flow out of the western boundary currents. This new feature of the circulation is characterized as a separated western region, where the solution is independent of the eastern boundary condition. Within this region, the nonlinear interaction between the wind-driven circulation and the buoyancy-forced circulation is very strong. This can be seen from the difference in upwelling velocity at the interface (Fig. 6b). Notice that the maximum vertical velocity at the interface is 0.25×10^{-4} cm s^{-1}, and this maximum upwelling velocity is reached at the middle of the subpolar basin. Therefore, the nonlinear interaction between the buoyancy and wind makes a contribution, which is basically the same order as the wind-stress curl and has the same sign.

This nonlinear interaction can be seen also by separating the horizontal velocity into two components. The first one is due to the wind-stress curl, as seen in Figs. 7a and 7b. The second one is due to buoyancy forcing, as seen in Figs. 7c and 7d. Compared with the solution in Figs. 2c and 2d, the warm outflow from the western boundary has substantially changed the buoyancy-forced component of the solution (especially in the western region), while in the rest of the model basin the interaction is relatively weak and the solution can be seen as a linear superposition of these two components.

Similar to the previous case, there is a loop of boundary currents around the edge of the basin, which is necessary to close the mass flux of the model ocean. Compared with the case of purely buoyancy forcing, the maximum mass flux in the western boundary is slightly increased to about 54.9 Sv, while the total amount of deep water formed in the model is increased to 42.9 Sverdrups. The increase in the western boundary mass flux indicates stronger recirculation due to the wind-driven gyres. This increase in the deep-water formation is due to the increase in upwelling in the subpolar basin, especially within the western region.

The interaction between the wind-driven and buoyancy-driven circulation can be seen much better from the vertical structure of the circulation in Fig. 8. There is a strong anticyclonic gyre and a weak cyclonic gyre in the upper layer, while there is only a single cyclonic gyre in the lower layer. In the present model, the vertical velocity at the interface is assumed to be upward everywhere except in the northeastern corner. Therefore, the model is not suitable for the case with downwelling in the interior. If, however, the Ekman pumping is

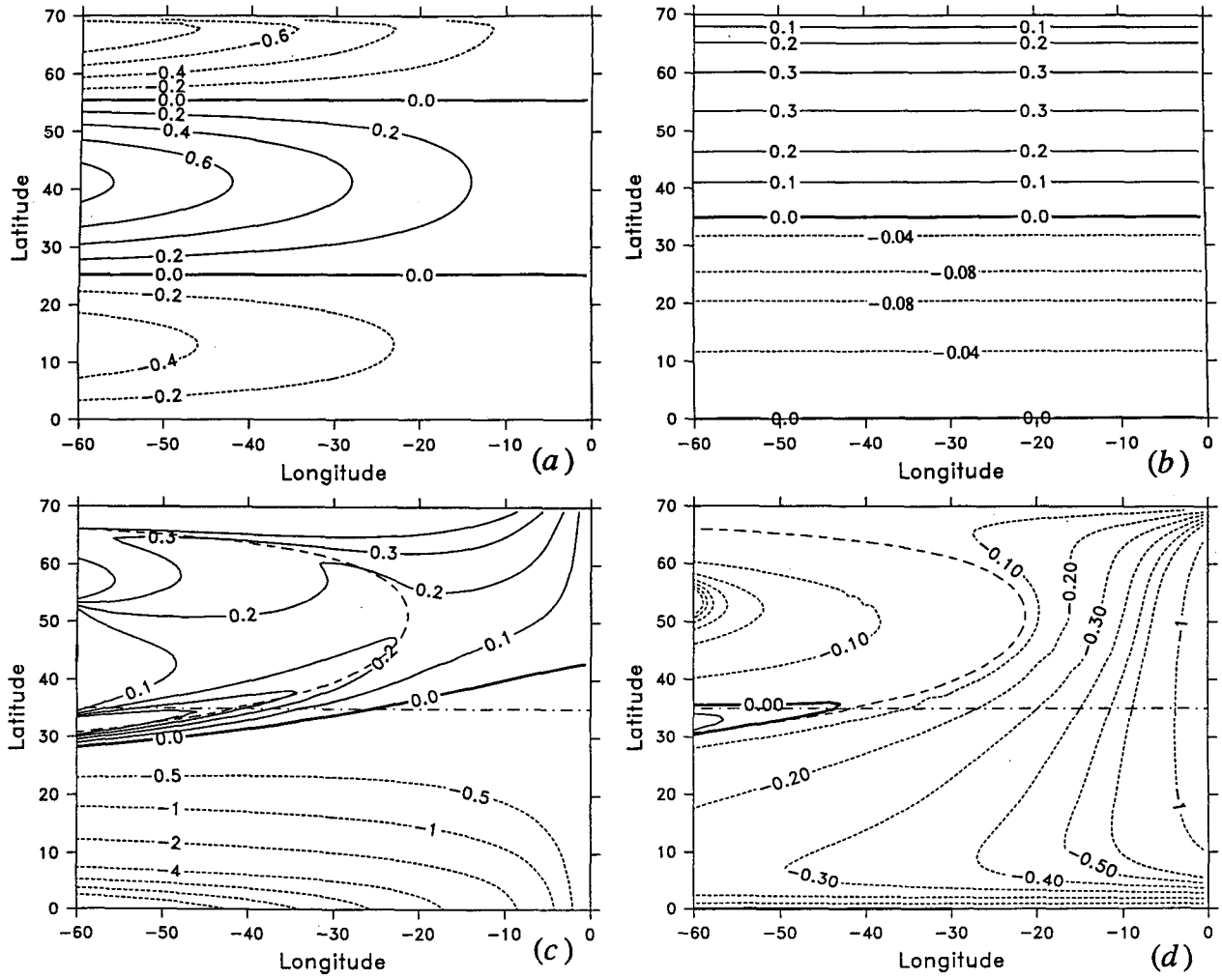

FIG. 7. Upper-layer zonal and meridional velocity components in centimeters per second. (a) Zonal velocity due to Ekman pumping, (b) meridional velocity due to Ekman pumping, (c) zonal velocity due to temperature gradient, and (d) meridional velocity due to temperature gradient.

stronger than what has been discussed here, downwelling may appear in the subtropical gyre. The cases with downwelling are interesting, but they cannot be studied using the present model.

Assuming there is basinwide interfacial upwelling, the lower layer is driven northward, and the upper layer southward. In the subtropical basin the Ekman pumping intensifies the southward flow in the upper layer and weakens the northward flow in the lower layer. In the subpolar basin the Ekman suction drives water northward, going against the thermal forcing, but it intensifies the northward flow in the lower layer. In the model, the upwelling is very strong in the subtropical basin, but the Ekman pumping is relatively weak. As a result, the circulation in the subtropical basin is predominantly thermally driven, so it has a very clear baroclinic structure. On the other hand, in the subpolar basin the wind-driven circulation is compatible with the buoyancy-driven circulation. The left-handed β spirals can be seen from this figure.

Luyten and Stommel (1986) introduced the concept of direct cell and indirect cells for the subpolar basin. The direct cell is characterized by a poleward motion in the upper layer and an equatorward motion in the lower layer, both driven by the interfacial downwelling. Since our model excludes the possibility of downwelling in the interior, no direct cell is possible in the model, and the whole subpolar gyre belongs to the indirect cell. The indirect cell, however, can be further divided into three regions, 1) a barotropic region in the middle and 2) two baroclinic regions, one in the east and one in the west. At the intergyre boundary these three regions join together at the Rossby repellor. In comparison, Pedlosky (1986) and Schopp (1988) discussed the case where a single baroclinic region exists east of the Rossby repellor. Although their solutions require

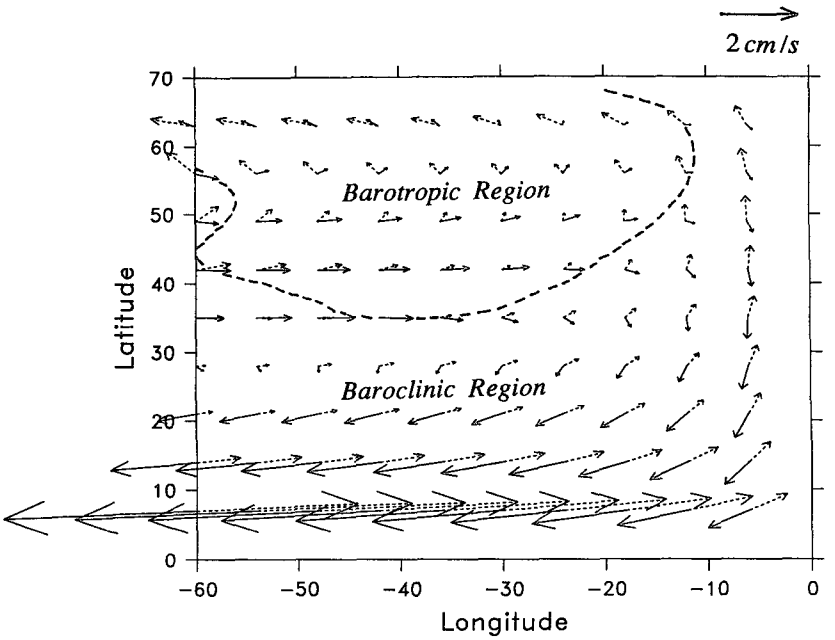

FIG. 8. Vector diagram for the upper-layer velocity (solid arrows) and lower-layer velocity (dashed arrows). The dashed line indicates the boundary between the barotropic and baroclinic regions.

no heating along the intergyre boundary, these baroclinic modes imply buoyancy forcing for their own existence.

Although only the layer-averaged horizontal velocity has been used in our calculations, the model can provide a three-dimensional structure of the velocity field. Within the lower layer there is no temperature gradient, so the meridional velocity is uniform and the vertical velocity is a linear function of depth. Since the horizontal temperature gradient is uniform in the upper layer, the meridional velocity has a linear profile, while the vorticity equation gives rise to a parabolic structure for the vertical velocity (see Fig. 9).

The model is driven by buoyancy forcing through the air–sea heat exchange. The strength of the air–sea heat flux is about 30 w m^{-2} (see Fig. 10). For the case of purely buoyancy forcing, heat is being absorbed by the ocean everywhere except a narrow strip near the northern wall, and the total heat flux from atmosphere to the ocean interior is about 0.618×10^{15} W. For the case with combined forcing, heat flux is from the ocean to the atmosphere for the major part of the subpolar basin. This heat loss to the atmosphere is due to the warm water outflow from the western boundary. Notice that the total area of heat loss is much smaller than that of heat gain. The total heat loss is only about 0.038×10^{15} W, while the total heat gain is about 0.583×10^{15} W. Thus, the net heat gain for the ocean interior is about 0.545×10^{15} W. Notice that the smaller heat gain in the case of combined forcing does not mean that the wind-driven circulation will reduce the heat exchange. It may be an artifact of assuming the same bottom-layer temperature for both cases; however, as discussed above, the bottom-layer temperature could be different.

5. Discussion

In order to highlight the essential elements of the oceanic general circulation a model with the simplest possible dynamics is set up. The model equations include geostrophy, hydrostatic equilibrium, incompressibility, and heat conservation. There are several new features in the model:

1) The interfacial upwelling is determined from internal dynamic balance of the model, instead of being specified a priori. The model shows strong upwelling along the eastern boundary and the southern boundaries, which is not inconsistent with observations and other more elaborate models.

2) The subpolar basin is separated into the western and eastern regions by a characteristic emanating from the Rossby repellor. Solutions in these two regions can have quite different natures. Both temperature and velocity are continuous across this boundary; however, for the parameters used in this study, this boundary is a vorticity front.

3) For the parameters used in this study, the Rossby repellor also serves as a pivot where three zones of the subpolar basin join together, including two baroclinic zones in the eastern and western basin and a barotropic zone sandwiched in between.

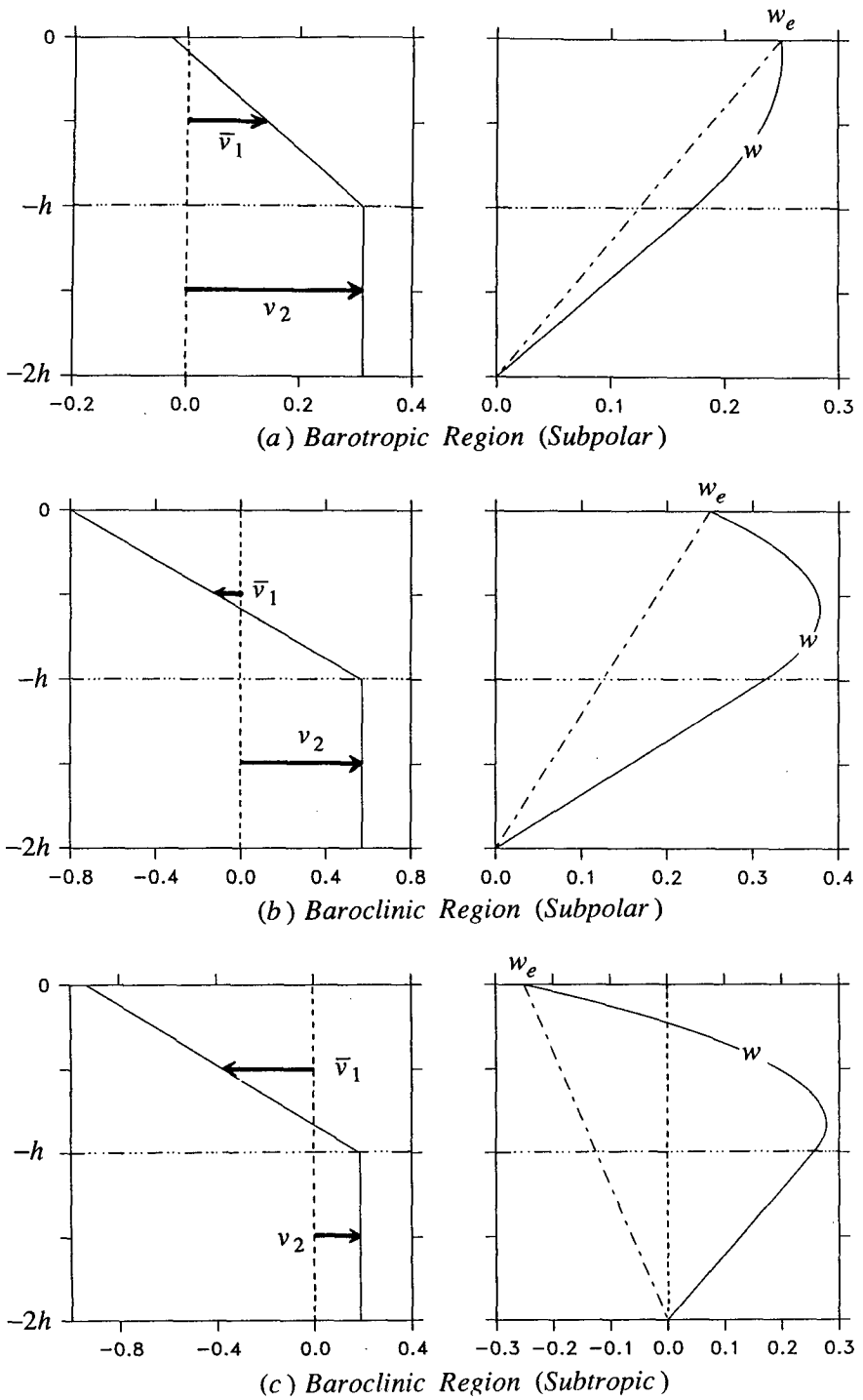

FIG. 9. Vertical profiles of the meridional and vertical velocity for the different regions of the model.

There is no horizontal diffusion in the model. As long as T_b and T_e are specified, the entire solution is determined. In fact, some important elements of the general circulation have been excluded from the model, such as deep-water formation and boundary currents around the western and northern edges of the basin. The deep-water formation process and these boundary currents, however, must play an essential role in setting up the right temperature for the deep water and the water along the eastern boundary.

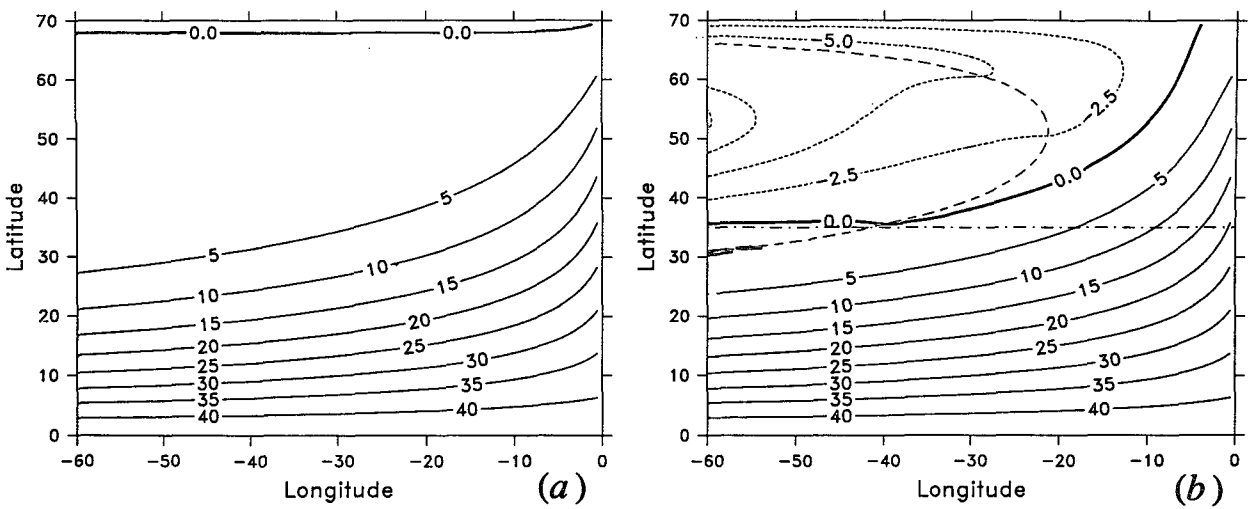

FIG. 10. Heat flux from the atmosphere to the ocean (W m^{-2}). (a) Without and (b) with Ekman pumping.

This study is a preliminary step toward understanding the three-dimensional structure of the thermohaline circulation in a basin. The ocean interior is basically an ideal fluid model with no horizontal diffusion, and the dynamics is simply the combination of thermal wind relation, hydrostatic equilibrium, and planetary vorticity equation. The success in obtaining a simple analytical or quasi-analytical solution is encouraging, and further study using a similar approach may lead to better understanding of the thermohaline circulation.

Acknowledgments. This study is the result of several conversations with Hank Stommel, to whom I am greatly indebted for suggestions and encouragement. An anonymous reviewer's comments were very helpful in clarifying the manuscript. This study was supported by grants from the Office of Naval Research, N00014-90-J-1518, and the National Science Foundation, OCE-9017158.

REFERENCES

Cushman-Roisin, B., 1984: On the maintenance of the subtropical front and its associated countercurrent. *J. Phys. Oceanogr.*, **14,** 1179–1190.

Haney, R. L., 1971: Surface thermal boundary condition for ocean circulation models. *J. Phys. Oceanogr.*, **1,** 241–248.

Huang, R. X., 1991: The three-dimensional structure of wind-driven gyres: Ventilation and subduction. U.S. national report to international union of geodesy and geophysics 1987–1990. *Rev. Geophys.*, 590–609.

Kawase, M., 1987: Establishment of deep ocean circulation driven by deep-water production. *J. Phys. Oceanogr.*, **17,** 2294–2317.

Killworth, P., 1985: A two-level wind and buoyancy driven thermocline model. *J. Phys. Oceanogr.*, **15,** 1414–1432.

Luyten, J. R., and H. Stommel, 1986: Gyres driven by combined wind and buoyancy flux. *J. Phys. Oceanogr.*, **16,** 1551–1560.

Pedlosky, J., 1986: The buoyancy and wind-driven ventilated thermocline. *J. Phys. Oceanogr.*, **16,** 1077–1087.

Schopp, R., 1988: Spinup toward communication between large oceanic subpolar and subtropical gyres. *J. Phys. Oceanogr.*, **19,** 1441–1452.

Stommel, H., and A. B. Arons, 1960: On the abyssal circulation of the world ocean—I. Stationary planetary flow patterns on a sphere. *Deep-Sea Res.*, **6,** 140–154.